Majorana fermions in noisy Kitaev wires

Ying Hu,[1] Zi Cai,[1] Mikhail A. Baranov,[1,2] and Peter Zoller[1,3]
[1]*Institute for Quantum Optics and Quantum Information of the Austrian Academy of Sciences, A-6020 Innsbruck, Austria*
[2]*NRC Kurchatov Institute, Kurchatov Square 1, 123182 Moscow, Russia*
[3]*Institute for Theoretical Physics, University of Innsbruck, A-6020 Innsbruck, Austria*
(Received 23 June 2015; published 16 October 2015)

Robustness of edge states and non-Abelian excitations of topological states of matter promises quantum memory and quantum processing, which are naturally immune to microscopic imperfections such as static disorder. However, topological properties will not in general protect quantum systems from time-dependent disorder or noise. Here we take the example of a network of Kitaev wires with Majorana edge modes storing qubits to investigate the effects of classical noise in the crossover from the quasistatic to the fast fluctuation regime. We present detailed results for the Majorana edge correlations, and fidelity of braiding operations for both global and local noise sources preserving parity symmetry, such as random chemical potentials and phase fluctuations. While in general noise will induce heating and dephasing, we identify examples of long-lived quantum correlations in the presence of fast noise due to motional narrowing, where external noise drives the system rapidly between the topological and nontopological phases.

DOI: 10.1103/PhysRevB.92.165118 PACS number(s): 05.30.Pr, 05.40.−a, 71.10.Pm, 03.65.Yz

I. INTRODUCTION

At present there is significant interest and ongoing effort in realizing and detecting topological phases of quantum matter in the laboratory [1–9]. These efforts are driven by both foundational aspects of our understanding of quantum ordered phases in many-body systems beyond the Landau paradigm of local order parameters (see, e.g., Refs. [10–12]), and in particular by the promises to use the intrinsic robustness of topological properties against imperfections in quantum information processing [13–17]. An example is provided by Kitaev's quantum wire [18] supporting a pair of Majorana edge modes—Majorana fermions—which show non-Abelian exchange statistics under braiding [19,20] and represent a topologically protected nonlocal zero-energy fermion. In a wire network, these properties can be used to create topologically protected qubits and gate operations [20]. The quest to demonstrate Majorana fermions and their non-Abelian properties is presently an outstanding challenge in quantum physics [21–24], and is the focus of a significant effort involving systems from hybrid nanowires [20,25–37] to cold-atom setups [38–46]. The first evidence for Majorana edge modes has been reported in recent experiments [31–37].

However, while the promise of topological protection of quantum states from microscopic imperfections may hold for static disorder (see, e.g., Refs. [15,16]), recent theoretical studies have concluded that Majorana qubits and braiding can be seriously affected by coupling to an environment [47–57], as will be the case in any realistic experimental scenario. The protection of Majorana modes in the Kitaev wire is related to protection of fermion parity, and quantum correlations between Majorana states will be rapidly destroyed by injection or removal of quasiparticles [49]. Even the coupling to a finite temperature bosonic bath, which preserves particle parity, is predicted to result in unavoidable losses of coherence and errors [56,57]. Nevertheless, as we will show in this paper, it is possible to identify examples with long-lived quantum correlations between Majorana states in the presence of noise. In particular, we will be interested in the effects of local and global noise representing a parity-preserving coupling to an environment, which we model as a classical stochastic process. The case of *local* noise is representative of a two-level fluctuator in a solid-state realization of a Kitaev wire [58], while *global* fluctuations can result, for example, from laser light fluctuations in cold-atom experiments.

Our goal is thus to study the effects of noise on Majorana correlations and braiding operations, in a regime ranging from quasistatic disorder, all the way to the limit of fast fluctuations, i.e., where the noise correlation time is much shorter than the relevant system time scales. Although coupling to classical noise will eventually always lead to dephasing and heating, dephasing can be suppressed in the fast fluctuation limit, even when the system is driven by the noise, e.g., between topological and nontopological phases. This effect of noise suppression with decreasing correlation time is familiar from atomic physics as motional narrowing. There, increasing the collision rate between atoms can result in a narrowing of the spectral lines [62], and in our context in an increased coherence time of Majorana correlations. In such cases, we will also determine the optimal conditions for braiding time scales—as a trade-off between the requirement of adiabaticity of braiding, and decoherence time scales.

The emphasis and value of the present work is on *exactly solvable* model quantum many-body dynamics of Majorana correlations and braiding operations in the presence of *colored Markovian noise* sources, as exemplified by telegraph noise, n-state jump models, or colored Gaussian noise. While in a solid-state context this should be understood as phenomenological models of noise describing imperfections such as local fluctuators, we note that noise in cold-atom experiments can be engineered, as in recent studies of Anderson localization with (static) random optical potentials [63,64]. Atomic realizations of Majorana fermions may thus serve as an ideal platform to study the effect of *time-dependent disorder* in a controlled setting by appropriate modulation of the laser beams to mimic various noise sources, and can thus provide a direct experimental counterpart to the present theoretical study.

The paper is organized as follows. In Sec. II, we briefly describe the model Hamiltonian of a noisy Kitaev wire. Then, in Sec. III, we develop techniques which allow nonperturbative solutions of the many-body quantum dynamics for colored Markovian noise with arbitrary correlation time. Based on these techniques, Sec. IV presents a study on the Majorana edge correlations and heating dynamics for a global noise, which stochastically drives the system, e.g., across the boundary between the topological and nontopological phases. The case of local noise is investigated in Sec. V. Thereafter, in Sec. VI, we study the effect of colored noise on Majorana transport, and discuss optimal conditions for Majorana manipulations to obtain the best fidelity at a given noise. The braiding dynamics on a noisy wire network is analyzed in Sec. VII, based on the noisy T-junction architecture and cold-atom setup, respectively. The paper closes with a summary and outlook in Sec. VIII.

II. NOISY KITAEV WIRE

Our goal is to study the dynamics of Majorana edge modes of the Kitaev wire in the presence of noise (see Fig. 1). The relevant Hamiltonian is

$$H[X(t)] = \sum_{j=1}^{N-1}[-J_j(t)a_j^\dagger a_{j+1} + \Delta_j(t)a_j a_{j+1} + \text{H.c.}] - \sum_{j=1}^{N}\mu_j(t)a_j^\dagger a_j, \quad (1)$$

where a_j and $a_j^\dagger$ are the operators of spinless fermions on a finite chain of N sites. Here $J_j(t)$ is the hopping amplitude on the lattice, $\Delta_j(t)$ is the pairing parameter, and $\mu_j(t)$ is the local chemical potential. We assume that these parameters fluctuate in time according to a given noise model $X(t) \equiv \{J_j(t), \Delta_j(t), \mu_j(t)\}$, which is motivated by a particular physical noise source related to a specific implementation. In hybrid nanowires the above Hamiltonian (or its continuous version) arises from a combination of spin-orbit coupling of electrons in the presence of a magnetic field, and the coupling to an s-wave superconductor [25–28,31–37]. Thus the effect of a two-level fluctuator, for example, can be represented by a fluctuating *local* chemical potential $\mu_j(t)$ on a given lattice site. On the other hand, a realization of the Kitaev wire with cold fermionic atoms in a 1D optical lattice results from a laser-induced coupling to a molecular Bose-Einstein condensate, where a molecule is dissociated into a pair of fermions in the wire, thus realizing the pairing term Δ_j [38,39,56]. Frequency fluctuations of the laser light can be understood as fluctuations of the laser detuning, or as a *global* fluctuating chemical potential $\mu_j(t) \equiv \mu(t)$.

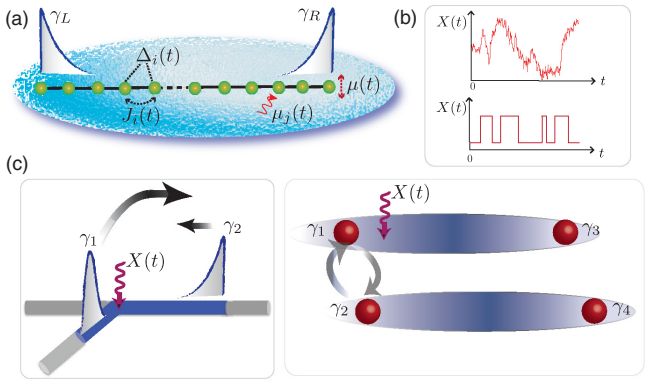

FIG. 1. (Color online) Schematic of Majorana edge modes in noisy Kitaev wires and braiding operations in the presence of colored Markovian noise. (a) A Kitaev wire in the topological phase supports two Majorana edge modes $\gamma_{L/R}$. In realistic implementations, a noisy Kitaev Hamiltonian (1) containing stochastic parameters $X(t) \equiv \{J_j(t), \Delta_j(t), \mu_j(t)\}$ arises, due to a coupling to a classical environment (blue background). The fluctuations can be either global [e.g., $\mu(t)$] or local [e.g., $\mu_j(t)$], depending on the physical sources of noise in specific implementations. (b) Two typical examples of colored Markovian noise $X(t)$: the colored Gaussian noise (upper panel) and the two-state telegraph noise (lower panel). (c) Braiding Majoranas (say, γ_1 and γ_2) on a noisy T junction in solid-state setting (left panel), and in a noisy atomic wire network in the optical lattice setup (right panel).

Before investigating the dynamics of the noisy wire (1), let us briefly describe as a reference the properties of a noise-free Kitaev's quantum wire [18], where $J_j(t) = J$, $\Delta_j(t) = \Delta$, and $\mu_j(t) = \mu$. When $|\mu| < 2J$ and $\Delta \neq 0$, the wire is in the topological phase characterized by a gapped energy spectrum in the bulk and by a pair of robust Majorana edge modes $\gamma_L = \gamma_L^\dagger$ and $\gamma_R = \gamma_R^\dagger$ of the form $\gamma_{L/R} = \sum_j f_{L/R,j}c_j$ [here we use the Majorana representation $c_{2j-1} = a_j + a_j^\dagger$ and $c_{2j} = -i(a_j - a_j^\dagger)$ of the operators] with $f_{L/R,j}$ being exponentially localized near the left (L) and right (R) edges with the localization length l_M. The pair of Majorana edge modes represents a nonlocal fermionic *zero-energy* mode $\alpha_M = (\gamma_L + i\gamma_R)/2$, and the long-range correlations $-i\langle\gamma_L\gamma_R\rangle$ between the Majorana edge states, which are of interest for us, are directly related to the occupation of this mode, $-i\langle\gamma_L\gamma_R\rangle = 1 - 2\langle\alpha_M^\dagger\alpha_M\rangle$. The robustness of the correlations is therefore related to the conservation of fermionic parity which distinguishes the two degenerate ground states with empty and occupied mode α_M. For $|\mu| > 2J$, when the wire is in the nontopological phase, there are no Majorana edge states and all excitations are gapped.

The presence of noisy components in the parameters of the Hamiltonian (1) results in random "shaking" of the system giving rise to changes in population of the α_M mode (accompanied by creation of bulk excitations) and, therefore, to the decay of the Majorana correlations. Large-amplitude global noise, say, in the chemical potential, can also drive the system across the quantum phase transition *between different phases*—topological and nontopological ones—i.e., between the cases with two Majorana edge modes and with none of them. Understanding the fate of Majorana edge modes, the correlations between them, and their braiding in the noisy Kitaev wire (1) involves the study of many-body nonequilibrium dynamics induced by the noise, and we describe the developed techniques for treating such problems in Sec. III.

III. QUANTUM DYNAMICS IN COLORED MARKOVIAN NOISE

In dynamics of quantum systems external noise appears as stochastic parameters in the Hamiltonian, as in Eq. (1),

and the time-dependent density matrix equation becomes a multiplicative stochastic differential equation [65,66]. Solving for the averaged density matrix in the presence of noise with arbitrary correlation times requires the development of nonperturbative techniques. For fast fluctuations, when the noise correlation time is much shorter than the system response time (white noise limit), a perturbative treatment, in the form of a lowest order cumulant expansion, results in a master equation for the stochastically averaged density matrix [65,66]. However, with increasing correlation time, the system response will be sensitive to all higher order correlation functions, and in the limit of infinite correlation time the static disorder problem is recovered (as in Anderson [67], and many-body localization [68]). In solving for quantum correlations and braiding dynamics in the noisy Kitaev wire we will rely on Markovian models of colored noise, which allow an exact solution of many-body dynamics for arbitrary correlation time of the noise.

At the heart of our solution of quantum dynamics for colored Markovian noise is the *generalized master equation* for the *marginal system density operator*. In brief, we assume a Markov process $X(t) \equiv \{X_\alpha(t)\}$, and we denote by $H[X(t)]$ the associated system Hamiltonian. Our goal is to solve the stochastic density matrix equation ($\hbar \equiv 1$), $\partial_t \rho(t) = -i[H[X(t)],\rho(t)]$, with $\rho(t)$ the density operator, for the stochastic average $\langle \rho(t) \rangle_s$ with angular brackets denoting the noise average. Defining a marginal density matrix

$$\rho(X,t) = \langle \rho(t)\delta(X(t) - X) \rangle_s, \tag{2}$$

we can derive the generalized master equation for the marginal density matrix (see Ref. [69] and Appendix A):

$$\partial_t \rho(X,t) = \mathcal{L}(X)\rho(X,t) - i[H(X),\rho(X,t)], \tag{3}$$

with X now a time-independent variable. Here $\mathcal{L}(X)$ is the generator of our Markovian noise model, as appears in the differential Chapman-Kolmogorov equation for the conditional density $P(X,t|X',t')$ [65]:

$$\partial_t P(X,t|X',t') = \mathcal{L}(X)P(X,t|X',t'). \tag{4}$$

Thus the operator $\mathcal{L}(X)$ provides a complete specification of our noise model, and appears as a damping operator in the generalized master equation (3). Solving (3) for $\langle \rho(t) \rangle_s = \int dX \rho(X,t)$ provides us with the desired average. We refer to Appendix B for a discussion of various limits of solving the above equation: this includes the regime of quasistatic disorder, and the fast fluctuation limit (master equation limit). We emphasize, however, that by solving (3) we obtain solutions valid for *arbitrary* correlation time.

The most general models for classical Markovian noises [65] are described by diffusion processes with continuous noise trajectory and by jump processes with $X(t)$ taking a set of discrete values $\{X_m\}$ ($m = 0,\ldots,N_r$). In the former case, $\mathcal{L}(X)$ corresponds to the Fokker-Planck operator, and a primary example is the colored Gaussian noise (Ornstein-Uhlenbeck process); see upper panel of Fig. 1(b). In the latter $\mathcal{L}(X)$ reduces to a matrix $\mathcal{L}_{mn}$ describing the jump rates between different X_m, as in the case of multistate telegraph noise; see lower panel of Fig. 1(b) for the two-state telegraph noise. While the solution for a diffusion process can in principle be obtained in terms of the eigenfunctions of the Fokker-Planck operator $\mathcal{L}(X)$ [65,69], we pursue here a much more convenient strategy by discretizing it to an N_r-state jump model with large N_r and properly chosen $\mathcal{L}_{mn}$—"putting the noise on a lattice." In this case the generalized master equation (3) takes on the form of a set of coupled equations for marginal density matrices $\rho(X_m,t)$

$$\partial_t \rho(X_m,t) = \sum_{n=0}^{N_r} \mathcal{L}_{mn}\rho(X_n,t) - i[H(X_m),\rho(X_m,t)], \tag{5}$$

which—at least for low-dimensional processes $X(t)$—is not significantly of more effort to solve than the original non-stochastic version.

Below we will illustrate the above techniques for the Markovian two-state jump model [see lower panel of Fig. 1(b)], which represents the simplest but relevant example capturing all essential features of noise dynamics. It also allows a straightforward extension to multistate jump models, or to noise from several fluctuators, which for a large number in the sense of the central limit theorem approaches colored Gaussian noise (see Appendix C). In addition, we will specialize the above equations to the case of a quadratic many-body Hamiltonian, as relevant for the Kitaev wire.

In two-state telegraph noise, the stochastic parameter $X(t)$ switches randomly between two discrete values a and b with rate κ. Equation (4) is now a rate equation for the probabilities $P(a,t)$ and $P(b,t)$ to be in state a or b, respectively:

$$\frac{d}{dt}\begin{bmatrix} P(a,t) \\ P(b,t) \end{bmatrix} = \begin{bmatrix} -\kappa & \kappa \\ \kappa & -\kappa \end{bmatrix}\begin{bmatrix} P(a,t) \\ P(b,t) \end{bmatrix} := \mathcal{L}\begin{bmatrix} P(a,t) \\ P(b,t) \end{bmatrix}. \tag{6}$$

We have $\langle X \rangle_s = (a+b)/2$ and $\langle X(t+\tau),X(t) \rangle_s = \sigma^2 \exp(-|\tau|/\tau_c)$ for the mean value and first-order correlation function, respectively, with $\tau_c = 1/2\kappa$ the correlation time and the variance $\sigma^2 = (a-b)^2/4$ (using the notation $\langle X,Y \rangle_s \equiv \langle XY \rangle_s - \langle X \rangle_s \langle Y \rangle_s$).

The dynamics of a Kitaev wire driven by a single telegraph noise can be readily derived in the Majorana representation, where the quadratic Hamiltonian (1) can be recast as $H[X(t)] = (1/4)\sum_{il} h_{il}[X(t)]c_i c_l$, with $h_{il} = -h_{li}$ being an asymmetric Hamiltonian matrix [18]. In the Majorana basis, the key quantity capturing the system dynamics is the covariance matrix $\langle \Gamma(t) \rangle_s = \mathrm{Tr}[\langle \rho(t) \rangle_s \hat{\Gamma}]$, with $\hat{\Gamma}_{il} = (i/2)[c_i,c_l]$. Thus from Eq. (5), we find for the marginal densities

$$\begin{aligned} \frac{d}{dt}\Gamma(a,t) &= -i[h(a),\Gamma(a,t)] - \kappa\Gamma(a,t) + \kappa\Gamma(b,t), \\ \frac{d}{dt}\Gamma(b,t) &= -i[h(b),\Gamma(b,t)] - \kappa\Gamma(b,t) + \kappa\Gamma(a,t). \end{aligned} \tag{7}$$

The desired stochastic average is $\langle \Gamma(t) \rangle_s = \Gamma(a,t) + \Gamma(b,t)$. Before proceeding with the general solution, we find it worthwhile to briefly comment on the fast and slow (quasistatic disorder) limit.

In the fast noise limit, when $1/\kappa$ is the shortest time scale, an adiabatic elimination of the fast dynamics in lowest order perturbation theory reduces the above equations to a master equation in Lindblad form,

$$\frac{d}{dt}\langle \Gamma \rangle_s = -i[h_+,\langle \Gamma \rangle_s] - \frac{1}{2\kappa}[h_-,[h_-,\langle \Gamma \rangle_s]], \tag{8}$$

with $h_\pm = [h(a) \pm h(b)]/2$. The first term describes a coherent evolution with the average Hamiltonian $h_+ \equiv \langle h \rangle_s$, while the second term is the noise-induced damping, which scales as $1/\kappa$. Suppression of the dissipation by fast noises is called motional narrowing in an atomic physics context [62], and corresponds to a Zeno effect [70]. If the *average* Hamiltonian is in the topological phase and thus supports Majorana edge modes, the initial Majorana correlation will show slow dephasing due to the Zeno effect—irrelevant if a or b *per se* lies in the topological or nontopological regime. On the other hand, in the limit of slow noise, i.e., when the jump rate $\kappa \to 0$, we can ignore $\mathcal{L}$ in Eqs. (3) and (7), $\mathcal{L} \to 0$, during long times $t \ll \kappa^{-1}$, so that for such times we simply have to perform the (quasi)static average of the system dynamics.

Below we will solve the full marginal density equations (7) for Majorana edge correlation $-i\langle \gamma_L \gamma_R \rangle_s = -\sum_{il} f_{L,i} f_{R,l} \langle \hat{\Gamma}_{il} \rangle_s$, with $f_{L/R,l}$ the Majorana wave function of the initial Hamiltonian in the Majorana basis. Our discussion will focus on the special case of local and global telegraph fluctuations of the chemical potential. As mentioned above, such telegraph noise can represent a local two-level fluctuator in a solid-state setup, and global laser frequency noise in an atomic realization of the Kitaev wires. We would like to stress, however, that even though we consider here the simplest jumplike noise process and only the chemical potential as a fluctuating parameter, our conclusions remain valid for a more general scenario with colored noise and with several fluctuating parameters.

We conclude this section with the remark that the considered Markovian noise models give rise to first-order noise correlation functions, which are exponentials, or superposition of exponentials. We note however that non-Markovian noise models can often be represented as projections of higher dimensional Markov processes, which can also be solved by our techniques. Another point to mention is that for nonquadratic Hamiltonians in one dimension, the generalized master equation (3) can be solved using the density matrix renormalization method [71,72], and the developed techniques therefore are interesting in a much broader context for many-body systems driven by colored noise.

IV. EDGE AND BULK DYNAMICS IN THE PRESENCE OF GLOBAL NOISE

We begin with discussing the time evolution of the Majorana edge correlation $-i\langle \gamma_L \gamma_R \rangle_s$ under the global fluctuations in the chemical potential $\mu(t)$, when it flips between two values μ_a and μ_b (the corresponding Hamiltonians are H_a and H_b, respectively) with the jump rate κ. The statistic property of $\mu(t)$ is described by the mean value $\mu_{\rm ave} = (\mu_a + \mu_b)/2$, the variance $\sigma^2 = (\mu_a - \mu_b)^2/4$, and the correlation time $\tau_c = 1/2\kappa$. We denote by $H_{\rm ave} = \langle H[\mu(t)] \rangle_s$ the average Hamiltonian over the noise realization, which in the considered case is of the form of a noise-free Kitaev Hamiltonian with $\mu = \mu_{\rm ave}$. For the initial condition, we take $\mu(0) = \mu_a$ with $|\mu_a| < 2J$ such that Hamiltonian H_a is in the topological phase, and assume the system is in the ground state with the Majorana edge-mode correlation $-i\langle \gamma_L \gamma_R \rangle = 1$. For the value μ_b, we consider three possible scenarios [see Fig. 2(a)]: (1) $|\mu_b| < 2J$, when the Hamiltonian H_b is in the topological phase (fluctuations within the topological phase); (2) $|\mu_b| > 2J$ but $|\mu_{\rm ave}| < 2J$, when H_b is in the nontopological phase but the average Hamiltonian $H_{\rm ave}$ remains in the topological phase (fluctuations between topological and nontopological phases but on average staying in the topological one); and (3) $|\mu_b| > 2J$ and $|\mu_{\rm ave}| > 2J$, when both Hamiltonians H_b and $H_{\rm ave}$ are nontopological (large-amplitude fluctuation when staying on average in the nontopological phase). The evolution of $-i\langle \gamma_L \gamma_R \rangle_s$ calculated on the basis of Eq. (7) for these three scenarios is shown in Figs. 2(b)–2(d), respectively, in the regimes of fast, intermediate, and slow jump rate κ.

We see that noise always leads to decay of Majorana correlations, but the decay dynamics significantly depends on the amplitude and rate of the noise. Not surprisingly, we find the slowest decay of the Majorana correlations in the scenario (1) when the fluctuating Hamiltonian always remains in the topological phase. Strikingly, the dynamics in the scenario (2) shows the same features, even though here we have jumps between topological and nontopological phases: In both scenarios, we observe the fastest decay in the regime with an intermediate jump rate [$\kappa = 0.7J$; black curves in Figs. 2(b) and 2(c)], when κ is comparable with the energy gap and the bandwidth ($\sim J \sim \Delta$) of the Hamiltonian H_a, whereas

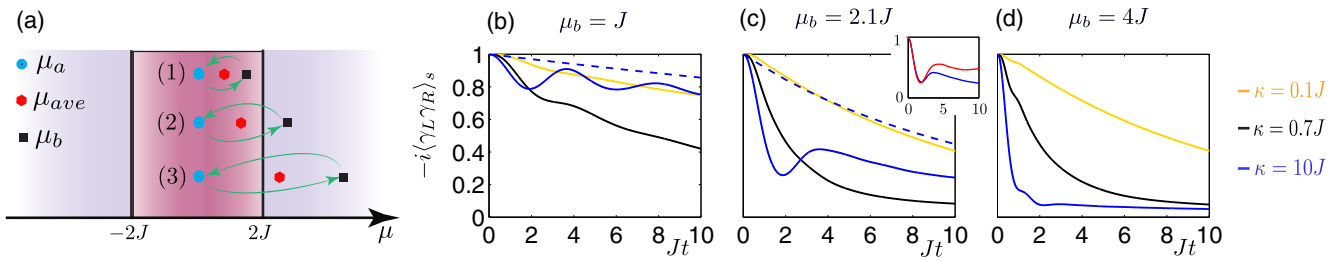

FIG. 2. (Color online) Evolution of Majorana edge correlations in the presence of a globally fluctuating chemical potential. (a) For a chemical potential $\mu(t)$ flipping between μ_a and μ_b, there exist three jump scenarios (1)–(3) in the phase diagram corresponding to the value of μ_b. (b)–(d) Time evolution of the Majorana edge correlation function $-i\langle \gamma_L \gamma_R \rangle_s$ for $\mu_a = 0.2J$ and (b) $\mu_b = J$, (c) $\mu_b = 2.1J$, and (d) $\mu_b = 4J$. In each scenario, we take three typical jump rates: $\kappa = 0.1J$, $\kappa = 0.7J$, and $\kappa = 10J$, and consider a Kitaev wire of $N = 60$ sites with the pairing parameter $\Delta = 0.8J$. We have considered two types of initial conditions, which correspond to the ground state of Hamiltonian H_a (solid curves) and of average Hamiltonian $H_{\rm ave}$ in the case of fast noises [blue dashed curves in (b) and (c)]. In the inset of (c), the dynamics for the noise with $\kappa = 10J$ (blue curve) for $\mu_b = 2.1J$ is compared with the quench dynamics (red curve), for a quench in the chemical potential from $\mu = 0.2J$ to $\mu = \mu_{\rm ave}$.

in both the slow ($\kappa = 0.1J$; yellow curves) and fast noise ($\kappa = 10J$; blue curves) regimes, the decay is much slower, and the system exhibits substantial Majorana correlations for much larger times ($>10J^{-1}$). In contrast to this nonmonotonic dependence on the noise rate, the decay rate in the scenario (3) grows with κ [see Fig. 2(d)]: for both intermediate and fast fluctuations there are no visible Majorana correlations for times $t \gtrsim 10J^{-1}$, although for slow noise they survive for a much longer time.

We now detail the analysis on the dynamical behavior of $-i\langle\gamma_L\gamma_R\rangle_s$ in scenarios (1)–(3) in the slow, fast, and intermediate regimes of the noise, respectively. We start with slow fluctuations when $\kappa \ll J \sim \Delta, \mu_{a(b)}$. In this case, the quenches between H_a and H_b—occuring at random instants—on average take place after a typical time κ^{-1}, which is much larger than all characteristic time scales of the system. As is explained in Appendix D, on the time scale of several inverse bandwidths of the system ($\sim J^{-1}$) after a quench, the Majorana correlations relax to asymptotic values which are determined by the overlap of the Majorana edge-mode wave functions for the Hamiltonians H_a and H_b. Such asymptotic values then remain constant till the next quench occurs. For the scenarios (2) and (3), when H_b is nontopological and has no edge modes, the overlap is zero, and already the first quench completely destroys the correlations. We therefore have $-i\langle\gamma_L\gamma_R\rangle_s \sim \exp(-\kappa t)$ for these scenarios [yellow curves in Figs. 2(c) and 2(d)]. On the other hand, for the scenario (1) when H_b has the zero mode, the overlap is nonzero. In this case, each quench reduces the correlations by a factor of $G_\infty < 1$ related to the overlap [see Eqs. (D1) and (D3) in Appendix D], resulting in a slower decay of the correlation $-i\langle\gamma_L\gamma_R\rangle_s \sim \exp[-\kappa(1-G_\infty)t]$ [yellow curve in Fig. 2(b)].

In the opposite regime of fast fluctuations ($\kappa \gg |\mu_b - \mu_a|$, $J \sim \Delta$), the dynamic behavior is remarkably related to the Zeno effect and to the quench problem. In this case, the evolution of $-i\langle\gamma_L\gamma_R\rangle_s$ can be explained based on Eq. (8) for the correlation matrix, which in the considered case takes the form

$$\frac{d}{dt}\langle\Gamma\rangle_s = -i[h_+,\langle\Gamma\rangle_s] - \frac{\sigma^2}{2\kappa}[N,[N,\langle\Gamma\rangle_s]]. \qquad (9)$$

Here $\sigma = |\mu_b - \mu_a|/2$ as mentioned earlier, and the matrices h_+ and N correspond to the Hamiltonian $H_{\rm ave}$ and the total particle number operator in the Majorana basis. Following from Eq. (9), we see the following:

(i) In the limit $\kappa \to \infty$, when the second "decay" term can be neglected, Eq. (9) describes the dynamics of correlations after the quench from the initial Hamiltonian H_a to the *averaged* one $H_{\rm ave}$. As a result, the asymptotic ($t \to \infty$) value of the Majorana correlation function $-i\langle\gamma_L\gamma_R\rangle_s$ is determined again by the overlap of the wave functions of the Majorana edge modes (see Appendix D), but now for the Hamiltonians H_a and $H_{\rm ave}$. For Hamiltonian $H_{\rm ave}$ in the nontopological phase [scenario (3)], there are no such modes, and after the quench $-i\langle\gamma_L\gamma_R\rangle_s$ decays to zero on the time scale of the order of the inverse bandwidth of $H_{\rm ave}$. For $H_{\rm ave}$ in the topological phase [scenario (1) with topological H_b and scenario (2) with *nontopological* H_b], this mode exists giving rise to a nonzero overlap and to a finite asymptotic value of the correlations after the quench.

(ii) For a large but finite κ, the second term in Eq. (9) adds a slow decay on top of the quench dynamics, providing the asymptotic behavior of $-i\langle\gamma_L\gamma_R\rangle_s$ shown in Figs. 2(b) and 2(c). The short-time ($t \lesssim J^{-1}$) behavior of the correlations, seen in the form of damped oscillations on these figures, is sensitive to the details of the band structures of H_a and $H_{\rm ave}$. In general, the "closer" these Hamiltonians are, the more pronounced are the oscillations, and the less destructive effect has the quench on $-i\langle\gamma_L\gamma_R\rangle_s$.

(iii) Note that Eq. (9) suggests the preparation of the initial Majorana correlations with respect to the edge states of the Hamiltonian $H_{\rm ave}$, not H_a, which is practically also more natural for fast fluctuations. In this case, the first term in Eq. (9) has no destructive effects, and $-i\langle\gamma_L\gamma_R\rangle_s$ shows slow decay due to the second term [dashed blue lines in Figs. 2(b) and 2(c)]. This slow decay of Majorana correlations in the presence of fast noises—even for a sufficiently large fluctuation amplitude outside the topological phase—is a direct consequence of the Zeno effect, which reduces the dynamics with fast fluctuating parameters to a weakly damped dynamics with the averaged Hamiltonian.

Finally, in the intermediate regime when the fluctuation rate is of the order of typical energy scales in the system, $\kappa \sim J \sim \Delta$, $\mu_{a(b)}$, one has optimal conditions for pumping excitations into the system (heating), leading to the fastest decay of the Majorana correlations. This can be seen by looking at the growth in the system energy under the action of noises. To illustrate this heating dynamics, we consider the case when $\mu(t)$ jumps between $\mu_a = \mu - \delta\mu$ and $\mu_b = \mu + \delta\mu$ (such that $\mu_{\rm ave} = \mu$) with a rate κ, focusing on the

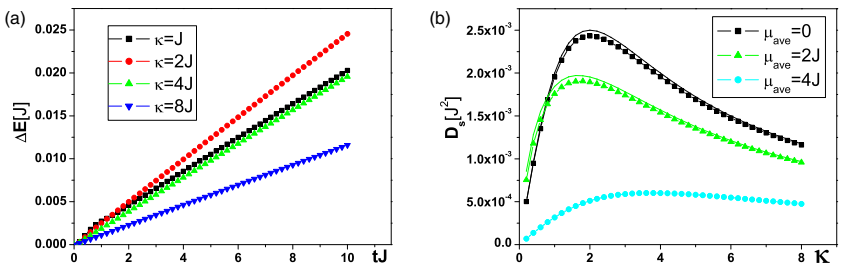

FIG. 3. (Color online) Heating dynamics in the bulk. (a) The absorbed energy $\Delta E(t)$ in units of J as a function of time for $\mu_{\rm ave} = 0$ and different κ. (b) Heating rate D_s in units of J^2 as a function of κ for different $\mu_{\rm ave}$. Numerical results (dotted curves) are compared to the predictions from Eq. (11) (solid curves). For (a) and (b), we have fixed the noise variance $\sigma = |\mu_b - \mu_a|/2 = 0.1J$, and have chosen $\Delta = J$.

weak noise limit $\delta\mu \ll J$ and choosing $\Delta = J$. We assume that initially the system is in the ground state of the *average* Hamiltonian $H_{\rm ave}$ [but still $\mu(t=0) = \mu_a$], with energy E_0 calculated with the corresponding initial density matrix $\rho_s(0)$, and calculate the system energy gain $\Delta E(t) = {\rm Tr}[\rho_s(t) H_{\rm ave}] - E_0$ for different μ and κ. A typical time evolution of $\Delta E(t)$ for different noise jump rates is shown in Fig. 3(a). There, the energy is seen to grow linearly, $\Delta E(t) = D_s t$, after a short transition time ($t \lesssim J^{-1}$). Then after a relatively long time (not shown) due to the small noise amplitude $\delta\mu \ll J$, it saturates to the asymptotic value which depends on μ but not on κ (infinite-temperature state). The heating rate D_s depends on both κ and μ. Figure 3(b) shows D_s as a function of the jump rate κ for the values of chemical potential $\mu = 0$, $2J$, and $4J$, which correspond to the topological, critical, and nontopological phases, respectively. We see that D_s is a nonmonotonic function of κ, which is small when noise is slow or fast (Zeno effect), and has a pronounced maximum for $\kappa \approx (2$–$4)J$. The maximum corresponds to the situation when the inverse noise correlation time $\tau_c^{-1} = 2\kappa$, which determines the frequency width of the noise correlation function, lies inside the band of bulk excitations (the exact position depends on the band structure).

The linear growth of the energy for the considered times can be understood by calculating the energy gain in the second-order perturbation theory ($\hbar \equiv 1$):

$$\Delta E(t) = \sum_\nu \varepsilon_\nu |M_\nu|^2 \left\langle \left| \int_0^t d\tau \exp(i\varepsilon_\nu \tau) \mu(\tau) \right|^2 \right\rangle, \qquad (10)$$

where M_ν is the matrix element of the number operator between the ground state and the excited state $|\nu\rangle$ with the energy $E_0 + \varepsilon_\nu$. For the considered global perturbation, $|\nu\rangle$ simply corresponds to the state with two single-particle excitations with momenta k and $-k$, and the energy $\varepsilon_\nu = 2E_p = 2\sqrt{(2J\cos pa + \mu)^2 + 4\Delta^2 \sin^2 pa}$ with a being the lattice spacing. Performing the time derivative and assuming the time t being larger than the noise correlation time $\tau_c = (2\kappa)^{-1}$, we obtain the following expression for D_s:

$$D_s = \sum_p 2E_p |M_p|^2 \int_{-\infty}^{\infty} d\tau \langle \mu(\tau)\mu(0)\rangle \exp(2iE_p\tau),$$

where the summation is over the Brillouin zone $p \in (-\pi/a, \pi/a]$. With the expression $|M_p|^2 = |u_p v_p|^2 = (\Delta^2 \sin^2 pa)/E_p^2$ for the matrix element and $\langle \mu(\tau)\mu(0)\rangle = \mu^2 + \sigma^2 \exp(-2\kappa|\tau|)$ for the noise correlation function, we finally obtain ($k = pa$)

$$D_s = 4\sigma^2 \int_{-\pi}^{\pi} \frac{dk}{2\pi} \frac{\kappa}{\kappa^2 + E_k^2} \frac{\Delta^2 \sin^2 k}{E_k}, \qquad (11)$$

for the energy-growth coefficient. The above expression is plotted as solid lines in Fig. 3(b) and is in very good agreement with numerical data.

V. LOCAL NOISE

We next discuss the effects of the local noise on the Majorana correlations $-i\langle \gamma_L \gamma_R \rangle_s$, which we model by adding a fluctuating part to the chemical potential on the site d,

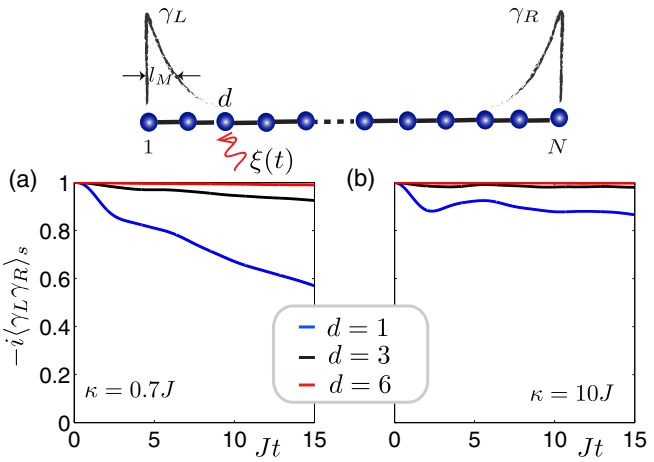

FIG. 4. (Color online) The effect of local noise at different locations in a Kitaev wire on Majorana edge correlations. (a) and (b) Time evolution of $-i\langle \gamma_L \gamma_R \rangle_s$ when a noise $\xi(t)$ arises in the local chemical potential at three different sites ($d = 1,3,6$), with a jump rate (a) $\kappa = 0.7J$ and (b) $\kappa = 10J$. We take $\xi_a = 0$ and $\xi_b = 0.8J$, $N = 60$, $\Delta = 0.4J$, and $\mu = 0.4J$. For this parameter choice, the localization length of the Majorana modes is $l_M \approx 2.5a$, with a being the lattice constant.

such that $\mu_j(t) = \mu + \delta_{j,d}\xi(t)$ with the amplitude $\xi(t)$ being described by the telegraph noise: $\xi(t)$ randomly flips between ξ_a and $\xi_b > 0$ with the rate κ, and $\xi(0) = \xi_a$. In this case, an exponential localization of the Majorana modes near the edges with the localization length l_M leads to a very strong dependence of the effects of the noise on d. This is because the decay of the Majorana correlations is caused by noise-induced changes in the population of the associated nonlocal fermionic zero-energy mode, with the corresponding matrix element being proportional to the value of the edge-mode wave function on the noisy site d. The results of our calculations for intermediate and fast noises, Figs. 4(a) and 4(b), respectively, clearly show this dependence: the decay is the fastest for $d < l_M$, for $d \sim l_M$ it is already substantially less, and is exponentially small for $d > l_M$.

Similar to the case of a global noise, the reduction of the decay in the fast-noise regime ($\kappa \gg J$, Δ, μ) is due to the Zeno effect, as follows from Eq. (8) which now takes the form

$$\frac{d}{dt}\langle\Gamma\rangle_s = -i[h_+, \langle\Gamma\rangle_s] - \frac{\sigma^2}{2\kappa}[n_d, [n_d, \langle\Gamma\rangle_s]],$$

where $\sigma = |\xi_b - \xi_a|/2$, the matrix n_d corresponds to the local density operator $a_d^\dagger a_d$ at site d in the Majorana basis, and the second term adds a slow decay on top of the result of the quench described by the first term. The average Hamiltonian in this case contains the *static* impurity potential $V_d = (\xi_a + \xi_b)/2$ on the site d, which results in just modification of the Majorana edge modes, and hence in a finite asymptotic value of $-i\langle \gamma_L \gamma_R \rangle_s$ after the quench. The small ($\sim\kappa^{-1}$) decay rate is extra reduced, as compared to the global noise, for $d \gtrsim l_M$ due to the smallness of the edge-mode wave functions on the site d. For $d > l_M$, this gives an exponentially small decay rate such that the Majorana correlations are practically immune to the noise (Fig. 4).

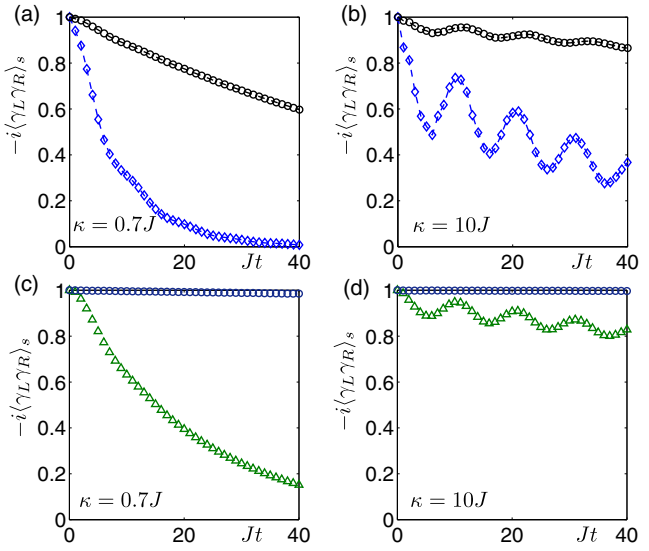

FIG. 5. (Color online) (a) and (b) The effect of a large-amplitude noise $\xi(t)$ in the local chemical potential on the dynamics of Majorana edge correlation $-i\langle\gamma_L\gamma_R\rangle_s$, when the local noise $\xi(t)$ arises at site $d = 3$ (blue curves) and $d = 6$ (black curves), flipping between $\xi_a = 0$ and $\xi_b = 4.4J$. (c) and (d) Evolution of the edge correlation $-i\langle\gamma_L\gamma_R\rangle_s$ when noise induces at random instants a splitting in the wire, between sites 3 and 4 (green curves) and between sites 6 and 7 (blue curves). In (a)–(d), we take two different noise jump rates, $\kappa = 0.7J$ (left panels) and $\kappa = 10J$ (right panels). Other parameters are the same as Fig. 4.

If we increase the amplitude of the noise to larger values, see Figs. 5(a) and 5(b) for $\xi_b = 4.4J$, the oscillating behavior for fast noise becomes much more pronounced. In this case, the strong static impurity potential in the average Hamiltonian splits the wire into two pieces which are weakly coupled through the impurity site (Josephson junction). If the coupling were zero, one would have an extra pair of Majorana modes at the edges adjacent to the impurity, and the corresponding fermionic zero mode. For a small but finite coupling, the energy of this mode is finite, and the oscillations seen in this case correspond to the energy of this mode. Similar oscillatory behavior is observed when the fast noise randomly splits the wire into two parts, for example, when the local hopping J_d and the pairing Δ_d amplitudes (between site d and $d + 1$) jump simultaneously between the finite values and zero, as shown in Figs. 5(c) and 5(d). In this case of fast noise, the average Hamiltonian has a "weak link," and the oscillation frequency seen in Fig. 5(d) corresponds to the energy of the fermionic mode localized at this link. Note that the amplitude of the oscillations is related to the overlap between the Majorana edge mode and the wave function of the low-energy fermionic mode localized on the "defected" site or link, and rapidly decreases with increasing distance between the modes.

Note that for the ideal Kitaev chain ($J = \Delta$ and $\mu = 0$), the two Majorana modes $\gamma_L = c_1$ ($\gamma_R = c_{2N}$) locate on the leftmost (rightmost) sites, such that $-i\langle\gamma_L\gamma_R\rangle_s = -(\Gamma_s)_{1,2N}$. In this case, the dynamics of the Majorana correlations is completely uncoupled from that of the bulk—the Majorana correlations in this ideal case are absolutely insensitive to what happens in the bulk.

VI. COMPETITION BETWEEN NOISE AND ADIABATICITY IN MAJORANA TRANSPORT

Equipped with above understanding of the nonequilibrium dynamics of a noisy Kitaev wire, we now discuss the effect of a local noise on the Majorana edge correlations during the adiabatic transport [20,29,30]—an essential building block for the braiding operations. As we will see, in the presence of a noise, the adiabaticity of the transport—required for preserving the information encoded in the Majorana correlations—confronts the finite lifetime of the correlations, and the competition of these two factors establishes an optimal operation time.

Following Ref. [20], we will move the left Majorana edge mode by "pushing" it to the right via adiabatically switching on local potentials on the corresponding sites. For example [see Fig. 6(a)], the move of γ_L from site 1 to site 2 can be achieved by applying the local potential $\lambda(t)V$ at site 1 [an extra term $\lambda(t)Va_1^\dagger a_1$ in the Hamiltonian], where $V \gg 2J$ and $\lambda(t)$ increases monotonically from $\lambda(t < 0) = 0$ to $\lambda(t > T_f) = 1$ during the time interval $[0,T_f]$ with T_f being much larger than the inverse energy gap, $T_f \gg J^{-1}$, Δ^{-1}, μ^{-1}. (In our

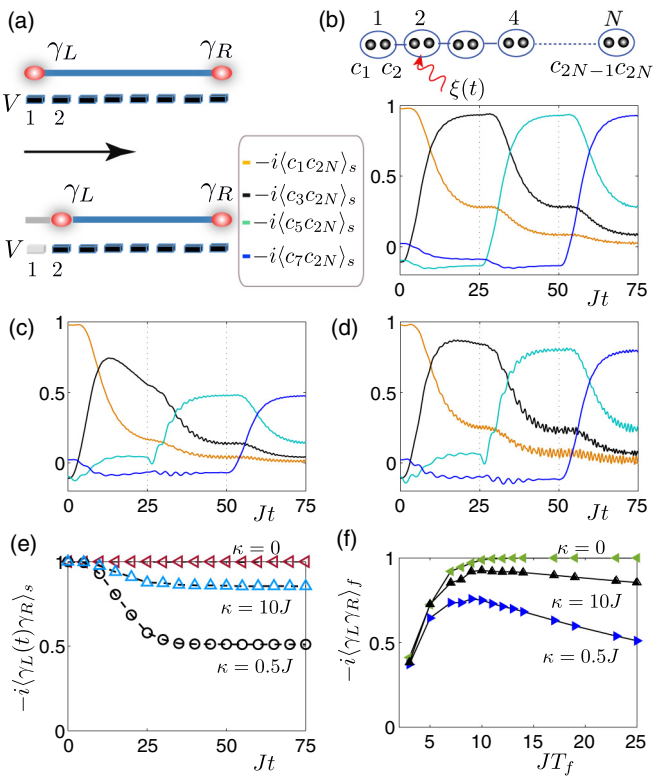

FIG. 6. (Color online) Fate of a Majorana moving through a local noise. (a) A move of the Majorana edge mode γ_L from site 1 to site 2 by adiabatically tuning the local potential V in a time interval T_f. (b)–(e) Time evolution of the correlation between the edge Majorana operators $-i\langle c_{2j-1}c_{2N}\rangle_s$ for $j = 1,2,3,4$, when γ_L is adiabatically transported from site 1 to site 4 through a local noise $\xi(t)$ at site $d = 2$ with (b) $\kappa = 0$, (c) $\kappa = 0.5J$, and (d) $\kappa = 10J$. (e) The time evolution of the correlations between the Majorana edge modes $-i\langle\gamma_L(t)\gamma_R\rangle_s$ for different κ. [$JT_f = 25$ for (b)–(e).] (f) The remaining Majorana correlations $-i\langle\gamma_L\gamma_R\rangle_f$ as a function of T_f for different κ, after γ_L is moved to site 4 (in total times of $3T_f$). For (b)–(f), we have chosen $\xi_a = 0$, $\xi_b = 0.8J$, $N = 40$, $\Delta = 0.8J$, and $\mu = 0.2J$.

calculations we use $\lambda(t) = \sin^2[(\pi/2T_f)t]$.) Further moves can be achieved by applying the same protocol successively to sites 2, 3, ... In Fig. 6(b) we show the evolution of the correlations $-i\langle c_{2j-1}c_{2N}\rangle$ with $j = 1,2,3,4$, during the adiabatic move of γ_L from site 1 to site 4 for $T_f = 25J^{-1}$ (in total time $3T_f$) and in the absence of the noise. [The correlation $-i\langle\gamma_L(t)\gamma_R\rangle$ between the actual edge modes remains unchanged from its initial value 1; see also the curve with $\kappa = 0$ in Fig. 6(e)].

The same correlations in the presence of the local noise $V_d[\xi(t)] = \xi(t)n_d$ at site d [here $\xi(t)$ flips again between ξ_a and ξ_b at a rate κ] are shown in Figs. 6(c) ($\kappa = 0.5J$) and 6(d) ($\kappa = 10J$) for $d = 2$. The corresponding behavior of the correlation $-i\langle\gamma_L(t)\gamma_R\rangle_s$ between the edge modes [$\gamma_L(t)$ is moving and γ_R is fixed] is presented in Fig. 6(e). We clearly see deviations from the noise-free case, which are significant for $\kappa = 0.5J$ and small for $\kappa = 10J$ (Zeno effect), but these deviations take place mostly when the Majorana mode moves to the noisy site (for t from 0 till T_f in the considered example). After that, the Majorana correlations do not exhibit any visible decay and repeat the pattern of the noise-free case but with the reduced amplitudes. This behavior follows from the localized character of wave functions of the Majorana edge states: the correlations between them are influenced by the local noise only when the moving Majorana mode and the noisy site are within the localization length l_M. (Note that the extent of the edge-mode wave function in the "nontopological" part of the wire—the sites with nonzero local potential V—is also nonzero but very small for $V \gg 2J$. As a result, a noisy site in this part of the wire has no effect on the correlations.)

The above results also imply that, in order to minimize the destructive effect of the noise on Majorana edge correlations, the move through the noisy site has to be performed with the fastest speed—the requirement which is opposite to the adiabaticity condition for the transport. As a result, there exists an *optimum speed* of transport (optimum T_f) for each κ. This is illustrated in Fig. 6(f) which shows the remaining correlations (after the total move) as a function of T_f for different κ: the decrease in the correlations for small T_f is due to nonadiabatic effects, while for large T_f it is due to accumulated action of the noise. The proper choice of T_f can substantially reduce the loss of correlations, especially in the intermediate-noise regime.

Similar consideration is also applicable to the global noise. However, in this case the destructive effect of the noise is independent of the position of the Majorana modes, so that an entire time of the operation should be within the lifetime of correlations; see Fig. 2.

VII. FIDELITY OF BRAIDING IN A NOISY WIRE NETWORK

Finally, we study the effects of the noise on the Majorana braiding (exchange)—the operation which for the two modes γ_1 and γ_2 corresponds (up to a phase) to the unitary operator $U = \exp[-(\pi/4)\gamma_1\gamma_2]$ and results in the transformation $\gamma_1 \to \gamma_2$, $\gamma_2 \to -\gamma_1$, showing the non-Abelian character of Majorana fermions [19,20]. We consider two proposed braiding scenarios: (i) in the T junction for the solid-state heterostructures, see Ref. [20], and (ii) in the wire networks for cold-atom systems, see Refs. [44,45].

We first consider the T junction with two Majorana edge modes $\gamma_1 = \gamma_L$ and $\gamma_2 = \gamma_R$ which we braid by moving them, see Fig. 7, in accordance with the protocol from Ref. [20]. We choose initially $-i\langle\gamma_1\gamma_2\rangle = 1$ and follow the evolution of this correlation during the protocol. Without noise, it remains unchanged during the entire braiding, provided we move the modes, say γ_1, adiabatically (we choose $T_f = 18J^{-1}$). In the presence of local noise, from the previous results we expect the decrease of $-i\langle\gamma_1(t)\gamma_2(t)\rangle_s$ each time when the Majorana mode passes the noise site. This is demonstrated in Fig. 7 for the case when the noise source is located at the common point of the three legs forming the T junction: here the Majorana modes have to cross the noisy site three times, and each crossing results in the decrease of $-i\langle\gamma_1(t)\gamma_2(t)\rangle_s$. For the noisy site located in one of the legs, only two crossings occur with the two corresponding drops in $-i\langle\gamma_1(t)\gamma_2(t)\rangle_s$, resulting in a higher fidelity of the braiding operation.

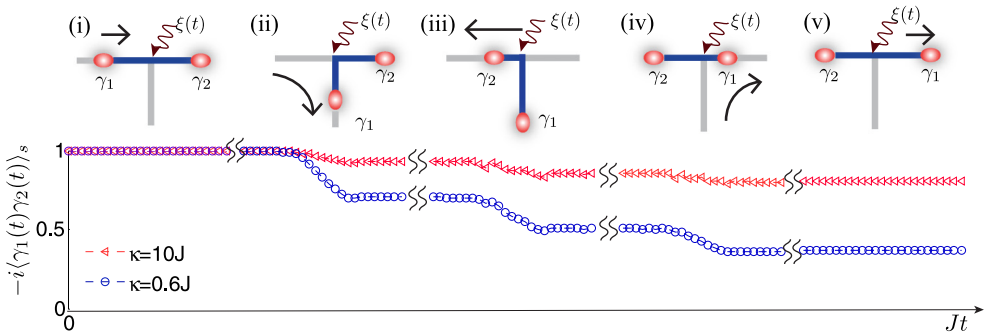

FIG. 7. (Color online) Majorana braiding on a noisy T junction, where a local noise $\xi(t)$ occurs in the common joint connecting three wire segments. Upper panel: Schematics of an exchange of two Majoranas γ_1 and γ_2 following Ref. [20]: (i) Initially the horizontal wire is topological supporting two Majorana edge modes γ_1 and γ_2 at the ends, while the vertical wire is nontopological. (ii) γ_1 is moved through the junction to the bottom of the vertical wire, while γ_2 is fixed at the right end of the horizontal wire. (iii) γ_2 is moved all the way to the left end of the horizontal wire, while γ_1 is fixed. (iv) γ_1 is moved upward through the junction and then rightward. (v) At the end of the exchange, the wire returns to its original configuration, with $\gamma_1 \to \gamma_2$ and $\gamma_2 \to -\gamma_1$. Lower panel: Evolution of the Majorana edge correlations $-i\langle\gamma_1(t)\gamma_2(t)\rangle_s$ in each step of the exchange processes, when a local noise $\xi(t)$ in the junction jumps between 0 and $0.7J$ at a jump rate $\kappa = 0.6J$ and $\kappa = 10J$, respectively. For other parameters, the pairing parameters of the horizontal and vertical wires are chosen as $\Delta_x = i\Delta_y = 0.7J$. We take $\mu = 0.1J$ in the topological segment and $\mu = -4J$ in the nontopological segment of the wires, and $JT_f = 18$.

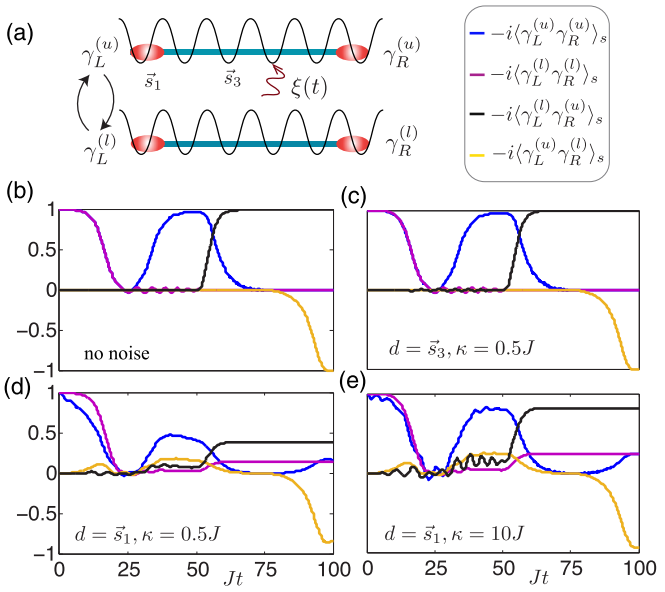

FIG. 8. (Color online) Braiding dynamics of Majoranas in a noisy atomic wire network. (a) Cold-atom implementation of braiding based on Refs. [44,45], where the Majorana modes $\gamma_L^{(u)}$ and $\gamma_L^{(l)}$ on the left ends of the two wires are exchanged. (b)–(e) Time evolution of the Majorana correlation functions for (b) noise-free case, (c) a local noise at site $\vec{s}_3$ of the upper wire with $\kappa = 0.5J$, and [(d) and (e)] a local noise at site $\vec{s}_1$ of the upper wire with (d) $\kappa = 0.5J$ and (e) $\kappa = 10J$. For (c)–(e), we choose $\xi_a = 0$ and $\xi_b = 0.6J$. For other parameters, $\Delta^{(u)} = \Delta^{(l)} = 0.7J$ and $\mu^{(u)} = \mu^{(l)} = 0$, $N^{(u)} = N^{(l)} = 32$. Following Refs. [44,45], the braiding is realized in four steps, where we choose the operation time t_f for each step as $Jt_f = 25$ for (b)–(e).

For the braiding in an atomic wire network, we consider two wires [see Fig. 8(a)]: the upper one (u) and the lower one (l), each having a pair of Majorana modes $(\gamma_L^{(u)},\gamma_R^{(u)})$ and $(\gamma_L^{(l)},\gamma_R^{(l)})$. The braiding protocol from Refs. [44,45] involves operations only on one side (say, left) of the network, and the modes to be braided, $\gamma_1 = \gamma_L^{(l)}$ and $\gamma_2 = \gamma_L^{(u)}$, are also located on the same side. As a result, the protocol will be only sensitive to noise located close to the left side of the network. Figure 8(b) shows the evolution of correlations between various Majorana modes during braiding in the absence of the noise. The evolution of the same correlations with the telegraphic-noise source with $\kappa = 0.5J$ on the third site ($\vec{s}_3$) and on the first site ($\vec{s}_1$) of the upper wire is presented in Figs. 8(c) and 8(d), respectively. The figures clearly show the above mentioned feature of the protocol. Notably, for a fast noise, even when the noise source is located on the first site $\vec{s}_1$, one has much less noise-induced decoherence whence higher fidelity; see Fig. 8(e).

VIII. CONCLUSIONS AND OUTLOOK

To summarize, we have studied the decoherence of Majorana edge correlations and braiding dynamics in colored Markovian noises preserving parity symmetry. Our analysis relies on a technique for solving quantum many-body dynamics when the system parameters undergo local or global fluctuations modeled by classical stochastic processes with arbitrary correlation time. Our studies on noisy Kitaev wires show that, while the noise always gives rise to the decay of the correlations between Majorana edge states, there are several parameter regimes where the lifetime of the correlations remains sufficient for quantum manipulations with Majorana fermions, even without error corrections. This includes the cases of slow global noise and generic local noise in the bulk, and in particular, the case of fast noise where decoherence can be suppressed due to motional narrowing, also known as the Zeno effect. These results further allow us to optimize the manipulation protocols of Majoranas in both the solid-state and cold-atom settings. Our presentation is for two-level telegraph noises in chemical potentials, but the essential features of noise dynamics are also seen in the colored Gaussian noises (the lattice model), and in other types of noises, e.g., the phase fluctuation in the pairing parameters.

The present study and the development of techniques to treat the effect of noise from static disorder to the rapid fluctuation limit should also be seen in the broader context of dynamics of correlations in an interacting many-body quantum system in the presence of random fluctuations. The effect of random fluctuations, either as spatial disorder or temporal noise, on the properties of quantum many-body systems is a long-standing and important problem. Spatial static disorder underlies phenomena such as Anderson localization, and quantum many-body localization-delocalization transition in the presence of interaction, with typically short-range correlations in the localized phase. The time-dependent random fluctuations introduce temporal decoherence and possible heating, resulting in finite temporal correlations. Whether the combination of random fluctuations and interparticle interactions could lead to some interesting long-range dynamics in the space-time domain is an open and intriguing question. The considered model, being formally quadratic, implicitly contains the effects of interparticle interactions in the form of a paring term which is responsible for the existence of the nontrivial topological phase with non-Abelian Majorana states. Due to topological protection, these states and the long-range correlations between them survive the static disorder, and, therefore, the considered model provides a simple and tractable example from a very special class of topological system, both interacting and noninteracting, with correlations robust against static disorder. The results of our paper provide therefore a possible scenario for behavior of such systems in the presence of a temporal noise.

ACKNOWLEDGMENTS

We acknowledge helpful discussions with A. J. Daley, H. Pichler, J. Budich, M. Heyl, P. Hauke, and T. Ramos. This project was supported by the European Research Council (ERC) Synergy Grant UQUAM, and the SpezialForschungs-Bereich (SFB) FoQuS, Austrian Science Fund (FWF Project No. F4016-N23). Y.H. acknowledges support from the Institut für Quanteninformation GmbH.

APPENDIX A: DERIVATION OF THE GENERALIZED MASTER EQUATION

Following Ref. [69], here we derive the generalized master equation (3) for the marginal density matrix $\rho(X,t)$ in the main text. Denoting $A[X(t)]\rho(t) \equiv -i[H[X(t)],\rho(t)]$,

for each noise realization we can solve the multiplicative stochastic equation $\dot{\rho}(t) = A[X(t)]\rho(t)$ for the density matrix $\rho(t)$ given an initial one $\rho(t_0)$ at t_0 with $X(t_0) = X_0$. The formal solution can be written as $\rho(t) = \sum_{n=0}^{\infty} \rho_n(t)$, with $\rho_n(t) = \int_{t_0}^{t} dt_n \ldots \int_{t_0}^{t_2} dt_1 \prod_{i=1}^{n} A[X(t_i)]\rho(t_0)$ for $t \geqslant t_n \geqslant \cdots \geqslant t_0$ and $\rho_0(t) = \rho(t_0)$. Thus from Eq. (2) we have $\rho(X,t) = \sum_{n=0}^{\infty} \rho_n(X,t)$ with $\rho_n(X,t) = \langle \rho_n(t)\delta(X - X(t))\rangle_s$, where the stochastic average can be straightforwardly performed using joint probability densities $P(X,t;X_n,t_n;\ldots;X_0,t_0)$. From the defining property of a Markov process, which is the factorization property of the conditional probability densities [65], we can write

$$\rho_n(X,t) = \int_{t_0}^{t} dt_n \ldots \int_{t_0}^{t_2} dt_1 \int dX_n \ldots \int dX_0 A(X_n) \ldots A(X_1)\rho(t_0)P(X,t|X_n,t_n)P(X_n,t_n;\ldots;X_0,t_0). \tag{A1}$$

Here $P(X,t|X_n,t_n)$ is the conditional probability for finding $X(t) = X$ given $X(t_n) = X_n$ at the earlier time $t_n < t$. The significance of Eq. (A1) is that the time dependence in the stochastic parameter $X(t)$ is now transferred into $P(X,t|X_n,t_n)$. Then by using the Chapman-Kolmogorov equation (4) for the evolution of $P(X,t|X',t')$ $(t' < t)$, together with $P(X,t|X',t) = \delta(X - X')$, we obtain

$$\dot{\rho}_n(X,t) = A(X)\rho_{n-1}(X,t) + \mathcal{L}(X)\rho_n(X,t), \tag{A2}$$

and $\dot{\rho}(X,t) = \sum_{n=0}^{\infty} \dot{\rho}_n(X,t)$ readily gives Eq. (3).

APPENDIX B: FAST FLUCTUATION AND QUASISTATIC LIMITS

Below we solve the generalized master equation (3) for the average density matrix $\rho_s(t) = \langle \rho(t)\rangle_s$ in two limiting cases of a stationary colored Markovian noise: (1) the fast fluctuation limit and (2) the quasistatic limit. (As above we will use the notation $A(X)\rho(X,t) = -i[H(X),\rho(X,t)]$.)

Fast fluctuation limit. In this case, a master equation for $\rho_s(t)$ can be derived using the eigenfunction expansion method [65,69]. Denoting the left (right) eigenfunctions of the noise operator $\mathcal{L}$ as $P_\lambda(X)$ $[Q_\lambda(X)]$, with $\mathcal{L}P_\lambda(X) = -\lambda P_\lambda(X)$ $[\mathcal{L}^\dagger Q_\lambda(X) = -\lambda Q_\lambda(X)]$, we expand

$$\rho(X,t) = \sum_\lambda P_\lambda(X)C_\lambda(t). \tag{B1}$$

Note that $P_0(X) = P_s(X)$ represents a stationary distribution with $\mathcal{L}P_s(X) = 0$, and $Q_0(X) = 1$. Denoting $(Q_\lambda, AP_{\lambda'}) = \int dX Q_\lambda(X)A(X)P_{\lambda'}(X)$ and using the orthogonal condition $(Q_\lambda, P_{\lambda'}) = \delta_{\lambda,\lambda'}$, the expansion coefficient $C_\lambda(t)$ in Eq. (B1) is derived as $C_\lambda = \int dX Q_\lambda(X)\rho(X,t)$. Importantly, we identify

$$\rho_s(t) = C_0(t) \equiv \int dX \rho(X,t), \tag{B2}$$

which is just the desired average density matrix.

We thus want to derive $\dot{\rho}_s = \dot{C}_0(t)$. Substituting Eq. (B1) into the generalized master equation (3), we find

$$\dot{\rho}_s = A_{\rm ave}\rho_s + \sum_{\lambda\neq 0}(Q_0, AP_\lambda)C_\lambda, \tag{B3}$$

$$\dot{C}_\lambda = -\lambda C_\lambda + (Q_\lambda, AP_0)\rho_s + \sum_{\lambda'\neq 0}(Q_\lambda, AP_{\lambda'})C_{\lambda'}, \tag{B4}$$

with $A_{\rm ave} = \int dX A(X)P_s(X)$. For fast fluctuations when the damping rate $\sim\lambda$ is large, we can eliminate the fast dynamics of $C_\lambda(t)$ [see Eq. (B4)] on a time scale $t \gg \lambda^{-1}$ using the technique of adiabatic eliminations [65]. In doing so, Eq. (B3) becomes (in linear order of $1/\lambda$)

$$\dot{\rho}_s(t) = (A_{\rm ave} + \mathcal{D})\rho_s(t). \tag{B5}$$

Here the operator $\mathcal{D}$ is defined by $\mathcal{D}\rho_s \equiv \int_0^t d\tau \langle A(\tau),A(0)\rangle_s \rho_s$, with $\langle A(\tau),A(0)\rangle_s = \sum_{\lambda\neq 0}[\int dX A(X)P_\lambda(X)]^2 e^{-\lambda\tau}$ the stationary variance [65] and $t \gg \lambda^{-1}$. Equation (B5) is the familiar master equation: the first term corresponds to a coherent evolution with the average Hamiltonian $H_{\rm ave}$; the second term describes a damping dynamics with the operator $\mathcal{D}$ determined only by the second-order noise correlations. As an illustration, consider $H[X(t)] = H_{\rm ave} + X(t)H_1$ [thus $A[X(t)] = A_{\rm ave} + X(t)A_1$]. For the example of noises $X(t)$ with exponential correlations, $\langle X\rangle_s = 0$ and $\langle X(\tau),X(0)\rangle_s = \sigma^2\exp(-|\tau|/\tau_c)$, we have $\mathcal{D} = \sigma^2\tau_c A_1 A_1$ for $t \gg \tau_c$ when Eq. (B5) becomes

$$\dot{\rho}_s = -i[H_{\rm ave},\rho_s] - \sigma^2\tau_c[H_1,[H_1,\rho_s]].$$

A similar equation arises in the main text in the concrete example of a fast two-state telegraph noise [see Eq. (8)].

Quasistatic limit. We now turn to the quasistatic case, when the relevant times (say, time for experimental observation) are much shorter than the noise correlation time, $t \ll \tau_c$. For this time the noise distribution is effectively frozen to the initial one, and hence we ignore $\mathcal{L}$ in Eq. (3) when it reduces to

$$\dot{\rho}(X,t) = -i[H(X),\rho(X,t)] \equiv A(X)\rho(X,t). \tag{B6}$$

Given an initial $\rho(X,0)$, the solution of Eq. (B6) gives the average density matrix for times $t \ll \tau_c$ as $\rho_s(t) = \int dX \exp[A(X)t]\rho(X,0)$ (valid to lowest order of τ_c^{-1}).

APPENDIX C: A LATTICE MODEL FOR COLORED GAUSSIAN NOISE

Here we present a lattice model for colored Gaussian noise $X(t)$ (Ornstein-Uhlenbeck process [65]), characterized by a mean value $\langle X(t)\rangle_s$ and a variance $\langle X(t+\tau),X(t)\rangle_s = \sigma^2\exp(-|\tau|/\tau_c)$. The basic idea is to form a multistate noise with N_r *independent* two-state telegraph noises: $X(t) = \sum_{r=1}^{N_r} X_r(t)$. Each telegraph $X_r(t)$ flips between a' and b' at a rate κ, with $\langle X_r\rangle_s = (a' + b')/2$ and $\langle X_r(t+\tau),X_{r'}(t)\rangle_s = \delta_{r,r'}\sigma'^2\exp(-\tau|/\tau_c)$. Here $\sigma'^2 = (a' - b')^2/4$ and $\tau_c = 1/2\kappa$ as in the main text. Thus by construction we have $\langle X(t)\rangle_s = N_r\langle X_r\rangle_s$, and $\sigma^2 = N_r\sigma'^2$. The noise $X(t)$ can be viewed as resulting from many independent two-level fluctuators with the same jump rate, so that the instantaneous value of $X(t)$ switches randomly among $N_r + 1$ discrete values $\{X_m\}$ $(m = 0,\ldots,N_r)$ with

$$X_m = ma' + (N_r - m)b'. \tag{C1}$$

We remark that, for *given* $\langle X(t)\rangle_s$ and σ of the noise $X(t)$, the values a' and b' of each telegraph are determined from scaling relations: $a' = \langle X(t)\rangle_s/N_r - \sigma/\sqrt{N_r}$ and $b' = \langle X(t)\rangle_s/N_r + \sigma/\sqrt{N_r}$.

The stochastic property of the above noise $X(t)$ is described by a probability density $P(X_m,t)$ for finding $X(t) = X_m$ at time

t, i.e.,

$$P(X_m,t) = \frac{m!}{(N_r-m)!N_r!}[P(a',t)]^m[P(b',t)]^{N_r-m}. \quad \text{(C2)}$$

Here $P(a'/b',t)$ is the probability for a telegraph being in state $a'(b')$ at time t with its evolution given by Eq. (7). Hence we obtain

$$\partial_t P(X_m,t) = \sum_{n=0}^{N_r} \mathcal{L}_{mn} P(X_n,t), \quad \text{(C3)}$$

with $\mathcal{L}_{m,m} = -\kappa N_r$, $\mathcal{L}_{m,m+1} = \kappa(m+1)$, $\mathcal{L}_{m,m-1} = \kappa(N_r - m + 1)$, and $\mathcal{L}_{m,n} = 0$ for $n \neq m, m \pm 1$.

For large N_r, the distribution (C2) approaches a Gaussian distribution as ensured by the central limit theorem [65], and Eq. (C3) represents the Fokker-Planck equation for an Ornstein-Uhlenbeck process [65]. To see this, we note that $X_{m+1} - X_m = b' - a' \sim 1/\sqrt{N_r}$ (with fixed σ of the noise), so that when $N_r \to \infty$ we can replace X_m with the continuous variable X and expand $P(X_{m\pm1})$ in terms of $\Delta X = b' - a'$ as $P(X \pm \Delta X) \approx P(X,t) \pm (b' - a')\partial_X P(X,t) + \frac{(b'-a')^2}{2}\partial_X^2 P(X,t)$. In view of $m = (N_r b' - X)/(b' - a')$ from Eq. (C1), we obtain from Eq. (C3) that

$$\partial_t P(X,t) = \left[2\kappa \frac{\partial}{\partial X}(X - \langle X\rangle_s) + \frac{1}{2} D \frac{\partial^2}{\partial X^2}\right] P(X,t).$$

This is the Fokker-Planck equation governing the Ornstein-Uhlenbeck process [65], where we identify a drift velocity 2κ, and a diffusion constant $D = 4\kappa\sigma^2$.

Thus the quantum dynamics of a system in (discretized) colored Gaussian noise is governed by the generalized master equation of a form (5) with X_m and $\mathcal{L}_{mn}$ given by Eqs. (C1) and (C3), respectively; for large N_r, it conveniently approximates Eq. (3) for a colored Gaussian noise when $\mathcal{L}(X)$ is the Fokker-Planck operator corresponding to an Ornstein-Uhlenbeck process.

APPENDIX D: ASYMPTOTIC LONG-TIME MAJORANA EDGE CORRELATIONS IN A QUENCHED KITAEV CHAIN

Here we derive the asymptotic Majorana edge-mode correlation at large times ($t \to +\infty$) after a global quench in the chemical potential of a Kitaev Hamiltonian, with the quench from μ_0 to μ_f. Specifically, we assume the system is initially in the ground state $|0\rangle$ of Hamiltonian $H(\mu_0)$ with $|\mu_0| < 2J$ in the topological phase, supporting two Majorana edge modes $\gamma_{L/R}$. Suppose at time $t = 0$, the Hamiltonian is globally quenched from $H(\mu_0)$ to $H(\mu_f)$ with $|\mu_f| \lesssim 2J$. Our goal is to derive the asymptotic ($t \to +\infty$) Majorana edge correlation

$$G_\infty = \lim_{t\to+\infty} \langle 0|e^{iH(\mu_f)t}[-i\gamma_L\gamma_R]e^{-iH(\mu_f)t}|0\rangle. \quad \text{(D1)}$$

In the Majorana basis, Eq. (D1) can be written as $G_\infty = \sum_{i,l=1}^{2N} f_{L,i}^{(0)} f_{R,l}^{(0)} G_{il}^\infty$, with $G_{il}^\infty = \lim_{t\to+\infty} -i\langle c_i c_l\rangle$, and $f_{L/R,l}^{(0)}$ describes left (right) Majorana modes of the initial Hamiltonian. As an illustration, we calculate G_{il}^∞ for $i = 2j_1 - 1$ and $l = 2j_2$ with $j_1 \sim 1$ (near the left edge) and $j_2 \sim N$ (near the right edge) such that $c_{2j_1-1} = a_{j_1} + a_{j_1}^\dagger$ and $c_{2j_2} = -i(a_{j_2} - a_{j_2}^\dagger)$. Using Bogoliubov transformation $a_j = \sum_\mu u_{j\mu}\beta_\mu + v_{j\mu}^*\beta_\mu^\dagger$, we diagonalize the postquench Hamiltonian $H(\mu_f)$ as $H(\mu_f) = \sum_\mu \epsilon_\mu \beta_\mu^\dagger \beta_\mu$ (up to unimportant constant) with β_ν being the quasiparticle operators for the Hamiltonian $H(\mu_f)$. With this we obtain $e^{iH(\mu_f)t} a_j e^{-iH(\mu_f)t} = \sum_\mu u_{j\mu}\beta_\mu e^{-i\epsilon_\mu t} + v_{j\mu}^*\beta_\mu^\dagger e^{i\epsilon_\mu t}$, and similarly for $e^{iH(\mu_f)t} a_j^\dagger e^{-iH(\mu_f)t}$. After substituting this into the expression for G_{il}^∞, and neglecting oscillating terms (the ones containing $\beta_\mu\beta_\nu$, $\beta_\nu^\dagger\beta_\mu^\dagger$, and $\beta_\mu^\dagger\beta_\nu$ with $\mu \neq \nu$) which are averaged to zero after times larger than inverse bandwidth, we obtain

$$G_{2j_1-1,2j_2}^\infty \approx -\sum_\mu \left(A_{j_1j_2\mu}\langle 0|\beta_\mu^\dagger\beta_\mu|0\rangle + B_{j_1j_2\mu}\langle 0|\beta_\mu\beta_\mu^\dagger|0\rangle\right),$$

with $A_{j_1j_2\mu} = (u_{j_1\mu}^* + v_{j_1\mu}^*)u_{j_2\mu} + (v_{j_1\mu} + u_{j_1\mu})u_{j_2\mu}^*$ and $B_{j_1j_2\mu} = (u_{j_1\mu} + v_{j_1\mu})v_{j_2\mu}^* + (v_{j_1\mu}^* + u_{j_1\mu}^*)v_{j_2\mu}$. To calculate the correlations in the above expression, we use the second Bogoliubov transformation $a_j = \sum_\sigma u_{j\sigma}^{(0)}\alpha_\sigma + v_{j\sigma}^{(0)*}\alpha_\sigma^\dagger$ which diagonalizes the initial Hamiltonian as $H(\mu_0) = \sum_\sigma \epsilon_\sigma \alpha_\sigma^\dagger\alpha_\sigma$ (again up to an unimportant constant) in terms of quasiparticle operators α_σ ($\alpha_\sigma^\dagger$), such that $\alpha_\sigma|0\rangle = 0$. Then, by virtue of the relation $\beta_\mu = \sum_\sigma C_{\mu\sigma}\alpha_\sigma + D_{\mu\sigma}^*\alpha_\sigma^\dagger$, with $C_{\mu\sigma} = \sum_j u_{j\mu}^* u_{j\sigma}^{(0)} + v_{j\mu}^* v_{j\sigma}^{(0)}$ and $D_{\mu\sigma} = \sum_j u_{j\mu}v_{j\sigma}^{(0)} + v_{j\mu}u_{j\sigma}^{(0)}$, we arrive at

$$G_{2j_1-1,2j_2}^\infty = -\sum_\mu \left(A_{j_1j_2\mu}\sum_\sigma |D_{\mu\sigma}|^2 + B_{j_1j_2\mu}\sum_\sigma |C_{\mu\sigma}|^2\right). \quad \text{(D2)}$$

Equation (D2) contains contributions from both the edge ($\mu = M$) and bulk modes ($\mu \neq M$) of $H(\mu_f)$ ($|\mu_f| \lesssim 2J$). Due to the gapped energy spectrum, the bulk contribution (modes with $\mu \neq M$) to the correlations between the edges are exponentially suppressed, and therefore can be ignored in Eq. (D2) in the thermodynamic limit. On the other hand, for the edge contribution ($\mu = M$), we use Majorana wave functions $g_{L/R,j}$ of Hamiltonian $H(\mu_f)$ in the fermionic representation: $g_{L,j} = u_{jM} + v_{jM}$ and $g_{R,j} = u_{jM} - v_{jM}$. Keeping in mind the localization character of the Majoranas at edges, we have $A_{j_1j_2M} \approx g_{L,j_1}g_{R,j_2}$ and $B_{j_1j_2M} \approx -g_{L,j_1}g_{R,j_2}$. Equation (D2) is then simplified as $G_{2j_1-1,2j_2}^\infty \approx g_{L,j_1}g_{R,j_2}\sum_\sigma(|C_{M\sigma}|^2 - |D_{M\sigma}|^2)$. This expression further involves contributions from the edge $\sigma = M$ and bulk modes $\sigma \neq M$ of initial Hamiltonian $H(\mu_0)$. For the same reasons discussed earlier, we ignore the exponential small bulk contributions ($\sigma \neq M$). For the rest edge contribution ($\sigma = M$), we write $u_{jM}^{(0)} = (1/2)(g_{L,j}^{(0)} + g_{R,j}^{(0)})$ and $v_{jM}^{(0)} = (1/2)(g_{L,j}^{(0)} - g_{R,j}^{(0)})$ with $g_{L/R,j}^{(0)}$ the initial Majorana wave functions of Hamiltonian $H(\mu_0)$ in the fermionic basis. Thus by using $C_{MM} = \frac{1}{2}\sum_j(g_{L,j}g_{L,j}^{(0)} + g_{R,j}g_{R,j}^{(0)})$ and $D_{MM} = \frac{1}{2}\sum_j(g_{L,j}g_{L,j}^{(0)} - g_{R,j}g_{R,j}^{(0)})$, we find

$$G_{2j_1-1,2j_2}^\infty \approx g_{L,j_1}g_{R,j_2}\left[\sum_{j=1}^N g_{L,j_1}g_{L,j_1}^{(0)}\right]\left[\sum_{j=1}^N g_{R,j_2}g_{R,j_2}^{(0)}\right].$$

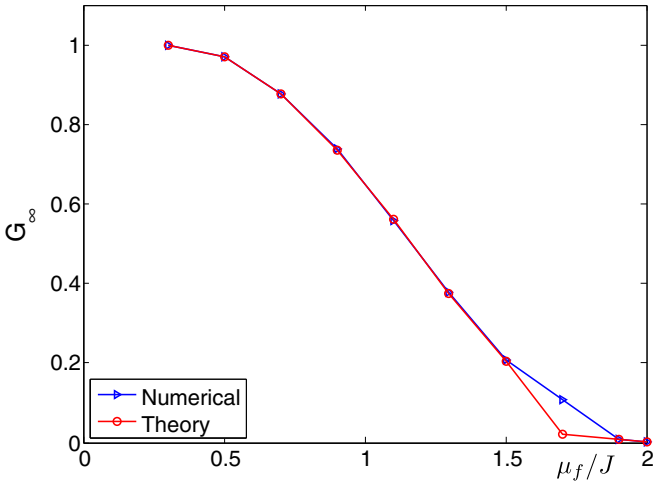

FIG. 9. (Color online) Long-time asymptotic Majorana edge-mode correlation G_∞ (D1) as a function of the postquench chemical potential μ_f, when a Kitaev Hamiltonian is globally quenched from $H(\mu_0)$ to $H(\mu_f)$, with $|\mu_0|,|\mu_f| \lesssim 2J$. Blue line, numerics; red line, Eq. (D3). We take $\mu_0 = 0.3J$, $N = 134$, $\Delta = 0.72J$.

Calculations of other components of G_{il}^{∞} are similar, and we finally get

$$G_\infty = \left[\sum_{j=1}^{N} g_{L,j} g_{L,j}^{(0)}\right]^2 \left[\sum_{j=1}^{N} g_{R,j} g_{R,j}^{(0)}\right]^2. \qquad \text{(D3)}$$

We see that, after the quench, the Majorana edge correlation in the long time approaches an asymptotic value, which is determined only by the overlap between the wave functions of the Majorana edge modes of $H(\mu_0)$ and $H(\mu_f)$ (i.e., $g_{L/R,j}^{(0)}$ and $g_{L/R,j}$). Figure 9 shows numerical results for G_∞ (blue curve) as a function of μ_f, which are compared to predictions from Eq. (D3) (red curve). A good agreement is clearly found, with deviations only appearing near the critical point when the energy gap becomes small. We thus conclude that Majorana edge correlations relax to a finite value after a quench within the topological phase, which decreases with μ_f in the postquench Hamiltonian and eventually varnishes for $\mu_f = 2J$.

[1] M. König, S. Wiedmann, C. Brüne, A. Roth, H. Buhmann, L. W. Molenkamp, X. L. Qi, and S. C. Zhang, Science **318**, 766 (2007).
[2] D. Hsieh, D. Qian, L. Wray, Y. Xia, Y. S. Hor, R. J. Cava, and M. Z. Hasan, Nature (London) **452**, 970 (2008).
[3] Y. L. Chen, J. G. Analytis, J. H. Chu, Z. K. Liu, S. K. Mo, X. L. Qi, H. J. Zhang, D. H. Lu, X. Dai, Z. Fang, S. C. Zhang, I. R. Fisher, Z. Hussain, and Z. X. Shen, Science **325**, 178 (2009).
[4] M. Atala, M. Aidelsburger, J. T. Barreiro, D. Abanin, T. Kitagawa, E. Demler, and I. Bloch, Nat. Phys. **9**, 795 (2013).
[5] N. Goldman, J. Dalibard, A. Dauphin, F. Gerbier, M. Lewenstein, P. Zoller, and I. B. Spielman, Proc. Natl. Acad. Sci. U.S.A. **110**, 6736 (2013).
[6] G. Jotzu, M. Messer, R. Desbuquois, M. Lebrat, T. Uehlinger, D. Greif, and T. Esslinger, Nature (London) **515**, 237 (2014).
[7] L. Duca, T. Li, M. Reitter, I. Bloch, M. Schleier-Smith, and U. Schneider, Science **347**, 288 (2015).
[8] M. Mancini, G. Pagano, G. Cappellini, L. Livi, M. Rider, J. Catani, C. Sias, P. Zoller, M. Inguscio, M. Dalmonte, and L. Fallani, Science **349**, 1510 (2015).
[9] B. K. Stuhl, H. I. Lu, L. M. Aycock, D. Genkina, and I. B. Spielman, Science **349**, 1514 (2015).
[10] X. G. Wen, *Quantum Field Theory of Many-Body Systems: From the Origin of Sound to an Origin of Light and Electrons* (Oxford University Press, New York, 2004).
[11] M. Z. Hasan and C. L. Kane, Rev. Mod. Phys. **82**, 3045 (2010).
[12] X. L. Qi and S. C. Zhang, Rev. Mod. Phys. **83**, 1057 (2011).
[13] A. Kitaev, Ann. Phys. **303**, 2 (2003).
[14] S. Das Sarma, M. Freedman, and C. Nayak, Phys. Rev. Lett. **94**, 166802 (2005).
[15] C. Nayak, S. H. Simon, A. Stern, M. Freedman, and S. Das Sarma, Rev. Mod. Phys. **80**, 1083 (2008).
[16] J. K. Pachos, *Introduction to Topological Quantum Computation* (Cambridge University Press, Cambridge, 2012).
[17] J. Alicea and A. Stern, Phys. Scr., T **164**, 014006 (2015).
[18] A. Kitaev, Phys.-Usp. **44**, 131 (2001).
[19] D. A. Ivanov, Phys. Rev. Lett. **86**, 268 (2001).
[20] J. Alicea, Y. Oreg, G. Refael, F. von Oppen, and M. P. A. Fisher, Nat. Phys. **7**, 412 (2011).
[21] F. Wilczek, Nat. Phys. **5**, 614 (2009).
[22] J. Alicea, Rep. Prog. Phys. **75**, 076501 (2012).
[23] C. W. J. Beenakker, Annu. Rev. Condens. Matter Phys. **4**, 113 (2013).
[24] S. Das Sarma, M. Freedman, and C. Nayak, arXiv:1501.02813v2.
[25] J. D. Sau, R. M. Lutchyn, S. Tewari, and S. Das Sarma, Phys. Rev. Lett. **104**, 040502 (2010).
[26] R. M. Lutchyn, J. D. Sau, and S. Das Sarma, Phys. Rev. Lett. **105**, 077001 (2010).
[27] J. Alicea, Phys. Rev. B **81**, 125318 (2010).
[28] Y. Oreg, G. Refael, and F. von Oppen, Phys. Rev. Lett. **105**, 177002 (2010).
[29] B. I. Halperin, Y. Oreg, A. Stern, G. Refael, J. Alicea, and F. von Oppen, Phys. Rev. B **85**, 144501 (2012).
[30] A. Romito, J. Alicea, G. Refael, and F. von Oppen, Phys. Rev. B **85**, 020502(R) (2012).
[31] V. Mourik, K. Zuo, S. M. Frolov, S. R. Plissard, E. P. A. M. Bakkers, and L. P. Kouwenhoven, Science **336**, 1003 (2012).
[32] M. T. Deng, C. L. Yu, G. Y. Huang, M. Larsson, P. Caroff, and H. Q. Xu, Nano Lett. **12**, 6414 (2012).
[33] L. P. Rokhinson, X. Y. Liu, and J. K. Furdyna, Nat. Phys. **8**, 795 (2012).
[34] A. Das, Y. Ronen, Y. Most, Y. Oreg, M. Heiblum, and H. Shtrikman, Nat. Phys. **8**, 887 (2012).
[35] H. O. H. Churchill, V. Fatemi, K. Grove-Rasmussen, M. T. Deng, P. Caroff, H. Q. Xu, and C. M. Marcus, Phys. Rev. B **87**, 241401(R) (2013).

[36] A. D. K. Finck, D. J. Van Harlingen, P. K. Mohseni, K. Jung, and X. Li, Phys. Rev. Lett. **110**, 126406 (2013).
[37] S. Nadj-Perge, I. K. Drozdov, J. Li, H. Chen, S. Jeon, J. Seo, A. H. MacDonald, B. A. Bernevig, and A. Yazdani, Science **346**, 602 (2014).
[38] L. Jiang, T. Kitagawa, J. Alicea, A. R. Akhmerov, D. Pekker, G. Refael, J. I. Cirac, E. Demler, M. D. Lukin, and P. Zoller, Phys. Rev. Lett. **106**, 220402 (2011).
[39] S. Nascimbène, J. Phys. B: At. Mol. Opt. Phys. **46**, 134005 (2013).
[40] M. Sato, Y. Takahashi, and S. Fujimoto, Phys. Rev. Lett. **103**, 020401 (2009).
[41] S. Diehl, E. Rico, M. A. Baranov, and P. Zoller, Nat. Phys. **7**, 971 (2011).
[42] C. V. Kraus, S. Diehl, P. Zoller, and M. A. Baranov, New J. Phys. **14**, 113036 (2012).
[43] C. V. Kraus, M. Dalmonte, M. A. Baranov, A. M. Läuchli, and P. Zoller, Phys. Rev. Lett. **111**, 173004 (2013).
[44] C. V. Kraus, P. Zoller, and M. A. Baranov, Phys. Rev. Lett. **111**, 203001 (2013).
[45] C. Laflamme, M. A. Baranov, P. Zoller, and C. V. Kraus, Phys. Rev. A **89**, 022319 (2014).
[46] A. Bühler, N. Lang, C. V. Kraus, G. Möller, S. D. Huber, and H. P. Büchler, Nat. Commun. **5**, 4504 (2014).
[47] G. Goldstein and C. Chamon, Phys. Rev. B **84**, 205109 (2011).
[48] J. C. Budich, S. Walter, and B. Trauzettel, Phys. Rev. B **85**, 121405 (2012).
[49] D. Rainis and D. Loss, Phys. Rev. B **85**, 174533 (2012).
[50] M. J. Schmidt, D. Rainis, and D. Loss, Phys. Rev. B **86**, 085414 (2012).
[51] F. Konschelle and F. Hassler, Phys. Rev. B **88**, 075431 (2013).
[52] M. S. Scheurer and A. Shnirman, Phys. Rev. B **88**, 064515 (2013).
[53] L. Mazza, M. Rizzi, M. D. Lukin, and J. I. Cirac, Phys. Rev. B **88**, 205142 (2013).
[54] T. Karzig, F. Pientka, G. Refael, and F. von Oppen, Phys. Rev. B **91**, 201102(R) (2015).
[55] T. Karzig, A. Rahmani, F. von Oppen, and G. Refael, Phys. Rev. B **91**, 201404(R) (2015).
[56] Y. Hu and M. A. Baranov, arXiv:1412.2547v3.
[57] F. L. Pedrocchi and D. P. DiVincenzo, Phys. Rev. Lett. **115**, 120402 (2015).
[58] Decoherence of a superconducting qubit due to coupling to a single two-state charge fluctuator, or to a set of them with distributed switching rates and couplings to the qubit, was considered, for example, in Refs. [59–61].
[59] A. Grishin, I. V. Yurkevich, and I. V. Lerner, Phys. Rev. B **72**, 060509(R) (2005).
[60] Y. M. Galperin, B. L. Altshuler, J. Bergli, and D. V. Shantsev, Phys. Rev. Lett. **96**, 097009 (2006).
[61] B. Cheng, Q. H. Wang, and R. Joynt, Phys. Rev. A **78**, 022313 (2008).
[62] P. Avan and C. Cohen-Tannoudji, J. Phys. B: At. Mol. Opt. Phys. **10**, 155 (1977).
[63] G. Roati, C. D'Errico, L. Fallani, M. Fattori, C. Fort, M. Zaccanti, G. Modugno, M. Modugno, and M. Inguscio, Nature (London) **453**, 895 (2008).
[64] J. Billy, V. Josse, Z. Zuo, A. Bernard, B. Hambrecht, P. Lugan, D. Clément, L. Sanchez-Palencia, P. Bouyer, and A. Aspect, Nature (London) **453**, 891 (2008).
[65] C. Gardiner, *Stochastic Methods: A Handbook for the Natural and Social Sciences* (Springer, Berlin, 2010).
[66] N. G. Van Kampen, Phys. Rep. **24**, 171 (1976).
[67] P. W. Anderson, Phys. Rev. **109**, 1492 (1958).
[68] A. Pal and D. A. Huse, Phys. Rev. B **82**, 174411 (2010).
[69] P. Zoller, G. Alber, and R. Salvador, Phys. Rev. A **24**, 398 (1981).
[70] P. Facchi and S. Pascazio, J. Phys. A: Math. Theor. **41**, 493001 (2008).
[71] A. J. Daley, C. Kollath, U. Schollwöck, and G. Vidal, J. Stat. Mech.: Theory Exp. (2004) P04005.
[72] U. Schollwöck, Rev. Mod. Phys. **77**, 259 (2005).